JCTC Journal of Chemical Theory and Computation

Article

pubs.acs.org/JCTC

Infrared and Raman Spectroscopy of Liquid Water through "First-Principles" Many-Body Molecular Dynamics

Gregory R. Medders and Francesco Paesani*

Department of Chemistry and Biochemistry, University of California, San Diego, La Jolla, California 92037, United States

Supporting Information

ABSTRACT: Vibrational spectroscopy is a powerful technique to probe the structure and dynamics of water. However, deriving an unambiguous molecular-level interpretation of the experimental spectral features remains a challenge due to the complexity of the underlying hydrogen-bonding network. In this contribution, we present an integrated theoretical and computational framework (named many-body molecular dynamics or MB-MD) that, by systematically removing uncertainties associated with existing approaches, enables a rigorous modeling of vibrational spectra of water from quantum dynamical simulations. Specifically, we extend approaches used to model the many-body expansion of interaction energies to develop many-body representations of the dipole moment and polarizability of water. The combination of these "first-principles" representations with centroid molecular dynamics simulations enables the simulation of infrared and Raman spectra of liquid water under ambient conditions that, without relying on any *ad hoc* parameters, are in good agreement with the corresponding experimental results. Importantly, since the many-body energy, dipole, and polarizability surfaces employed in the simulations are derived independently from accurate fits to correlated electronic structure data, MB-MD allows for a systematic analysis of the calculated spectra in terms of both electronic and dynamical contributions. The present analysis suggests that, while MB-MD correctly reproduces both the shifts and the shapes of the main spectroscopic features, an improved description of quantum dynamical effects possibly combined with a dissociable water potential may be necessary for a quantitative representation of the OH stretch band.

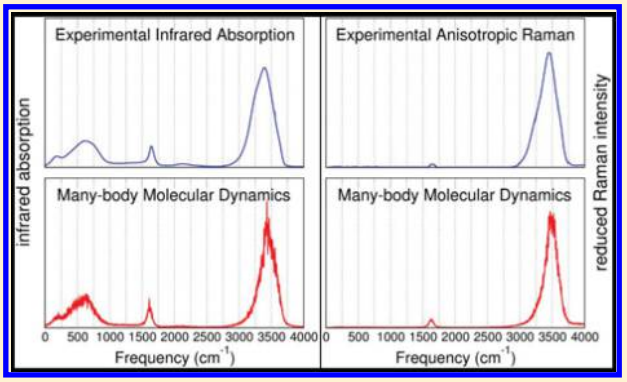

1. INTRODUCTION

From biological function to the Earth's climate, water is a key mediator of many natural phenomena.[1] To a large extent, this is related to the ability of the water molecules to form flexible and dynamic networks of hydrogen bonds. For example, hydration processes facilitated by the rearrangement of the water hydrogen-bonding network play a central role in the organization of ions at environmentally relevant interfaces,[2,3] in monolayer assembly,[4,5] in biological processes,[6−9] and in the stability and viability of novel materials for energy applications.[10,11]

Since the vibrational frequencies of a water molecule are particularly sensitive to the surrounding environment, vibrational spectroscopy has become a powerful tool for characterizing both molecular structure and dynamics of aqueous systems from the gas to the condensed phases.[5,11−18] However, a unique assignment of the spectra measured for water under different conditions and in different environments is nontrivial due to the fluctuating behavior of the underlying hydrogen-bonding network, which gives rise to several (homogeneously and/or inhomogeneously broadened) features that are often difficult to interpret. This has led to numerous controversies, including those about the nature of association bands,[19−21] the role of Fermi resonances, and the relationship between structural order and spectroscopic features at the air/water interface.[17,22−26] The theoretical interpretation of the water vibrational spectra has, in part, been complicated by the existence of numerous molecular models, which can provide conflicting explanations for the same spectroscopic features. In an attempt to overcome current theoretical limitations, we present here a unified many-body molecular dynamics (MB-MD) simulation approach developed exclusively from first principles to calculate vibrational spectra of water at a quantum-mechanical level.

Briefly, for a vibration to be infrared or Raman active, the charge distribution or polarizability must, respectively, change upon vibration.[27,28] Within the dipole approximation, this leads to the familiar selection rules for the fundamental adsorption intensities

$$I_{\mathrm{IR}}(\omega) \sim |\langle 1|\mu|0\rangle|^2 \tag{1}$$

and

$$I_{\mathrm{Raman}}(\omega) \sim |\langle 1|\alpha|0\rangle|^2 \tag{2}$$

Received: December 16, 2014
Published: February 13, 2015

DOI: 10.1021/ct501131j
J. Chem. Theory Comput. 2015, 11, 1145−1154

where μ is the dipole moment, α is the dipole−dipole polarizability (which, from this point forward, will be referred to simply as the polarizability), and the angular brackets represent integrals over the 0 and 1 vibrational levels. For condensed phase systems, where it is difficult to define the vibrational eigenstates, infrared and Raman spectra can be obtained within linear response theory through a more convenient time-dependent representation involving Fourier transforms of the corresponding quantum time-correlation functions, namely

$$I_{\mathrm{IR}}(\omega) \sim \int_{-\infty}^{\infty} \mathrm{d}t e^{-i\omega t} \langle \mu(0)\mu(t) \rangle \tag{3}$$

and

$$I_{\mathrm{Raman}}(\omega) \sim \int_{-\infty}^{\infty} \mathrm{d}t e^{-i\omega t} \langle \alpha(0)\alpha(t) \rangle \tag{4}$$

where the angular brackets imply an ensemble average. Through the time-dependent formulation presented in eqs 3 and 4, it is thus possible to identify three different elements that are necessary for a rigorous calculation of vibrational spectra: (1) a simulation approach capable of correctly describing the quantum dynamics of the system of interest, (2) an accurate representation of the underlying (Born−Oppenheimer) potential energy surface entering the Hamiltonian that governs the system dynamics, and (3) accurate representations of the multidimensional dipole moment and polarizability surfaces as a function of the system's degrees of freedom.

By far, the most common approach to solving eqs 3 and 4 is to approximate them through their classical counterparts. Classical correlation functions can be easily obtained from classical molecular dynamics (MD) simulations. For liquid water under ambient conditions, classical spectra describe the low-frequency (least quantum-mechanical) vibrations reasonably well,[29−34] but they predict relatively large blue shifts for the high-frequency (more quantum-mechanical) vibrations, such as the OH stretch[35,36]

Methods that attempt to directly obtain quantum time-correlation functions for condensed-phase systems can be classified in two main groups. The first group contains methods that treat quantum mechanically only a subset of the system's vibrations, with all remaining degrees of freedom being described at the classical level.[37−43] These mixed QM/MM methods have been extensively applied to model vibrational spectra of isotopically dilute solutions of HOD in H_2O (D_2O),[40,44,45] where, because of large frequency separations, the OD (OH) stretch of HOD can be considered to be effectively decoupled from all other vibrations in the system. Although mixed QM/MM methods have been successful in reproducing the OD (OH) line shape of HOD in H_2O (D_2O), recent ultrafast spectra measured for HOD in D_2O have demonstrated that the OH stretch of HOD is not fully decoupled from the other degrees of freedom.[46]

The second group of methods attempts to treat all nuclear degrees of freedom quantum mechanically by extending Feynman's path-integral formulation of statistical mechanics to dynamical properties. One of the first and more common approaches belonging to this group is centroid molecular dynamics (CMD), which, building upon path-integral molecular dynamics (PIMD), approximates the exact quantum dynamics in terms of classical-like equations of motion for the centroids of Feynman's ring-polymers.[47,48] Depending on the shape of the underlying potential energy surface, CMD may suffer from the so-called curvature problem, which can limit its applicability to molecular clusters and low-temperature condensed-phase systems.[49,50] However, it has been demonstrated that for water under ambient conditions the curvature problem is negligible, with IR spectra obtained from CMD being in very good agreement with those obtained from mixed QM/MM methods.[36,50,51] With the same spirit as CMD, ring-polymer molecular dynamics (RPMD) was subsequently introduced as an *ad hoc* approach to extending PIMD to the calculation of dynamical properties.[52] Vibrational spectra of water calculated from RPMD are contaminated by spurious resonances of the ring-polymer lying within the frequency window of the OH stretch.[53] A thermostatted version of ring-polymer molecular dynamics (TRPMD) has also been proposed, which removes the spurious resonances from the spectral region of interest by thermostatting the normal modes of the ring-polymers.[54] A systematic analysis of the OH line shape of HOD in D_2O has recently shown that the line shape predicted by TRPMD is significantly broader and somewhat blue shifted relative to the corresponding mixed QM/MM results.[36]

Regardless of the simulation method used to evaluate the relevant quantum time-correlation functions, a potential energy surface (PES) must be defined. For the case of liquid water, innumerable models of varying degrees of empiricism have been developed. A systematic comparison of the accuracy with which different models describe the Born−Oppenheimer PES for water was reported by us through a detailed analysis of the corresponding many-body expansion of interaction energies.[55] Among existing water models, our many-body potential with explicit polarization, MB-pol,[56,57] has been shown to accurately reproduce both structures and energetics of small clusters,[56,57] as well as thermodynamic and dynamical properties of bulk water under ambient conditions.[58] Improving upon other many-body potentials (e.g., CC-pol,[59−63] WHBB,[41,64] and HBB2-pol[55,65]), MB-pol was derived entirely from a large data set of highly correlated many-body interaction energies using machine learning techniques and employing mathematical functions that are sufficiently flexible to capture the multidimensional complexity of the reference electronic structure data.

The third element needed to solve eqs 3 and 4 are the system's dipole moment and polarizability surfaces. In MD simulations with empirical (nonpolarizable and polarizable) potentials, the dipole moment and polarizability of the water molecules can be easily calculated from the corresponding parameters defined within the model.[31,66−70] In the case of *ab initio* simulations, the system's dipole moment and polarizability can be obtained from the electronic density.[32,33,71−75] Within the MB framework, the many-body potential used in the actual MD simulations does not contain any information about the distribution of the electron density and the dependence of the energy on external electric fields. For this reason, many-body potentials cannot, in principle, be used to derive electrostatic properties, such as the system's dipole moment and polarizability, which are required for modeling IR and Raman spectra. While MB potentials employ some form of polarizable electrostatics to describe higher-order molecular interactions, the energy arising from this approximate electrostatics model is corrected with functions (e.g., permutationally invariant polynomials in the case of WHBB,[41,64] HBB2-pol,[55,65] and MB-pol[56−58]) that account for quantum-mechanical effects neglected by purely polarizable models, including correlation,

DOI: 10.1021/ct501131j
J. Chem. Theory Comput. 2015, 11, 1145−1154

exchange, charge penetration, and charge transfer. While these effects clearly affect both the charge distribution and polarizability, the extent to which these contributions affect the infrared and Raman vibrational spectra of liquid water is less clear. It is interesting to note that the same reasoning should be extended to empirical water models, in which partial charges and/or atomic polarizabilities, which are primarily fitted to reproduce structural and thermodynamic properties of the system of interest, do not necessarily have a rigorous connection to the underlying multidimensional dipole moment and polarizability surfaces.[76]

In this study, we introduce accurate, "first-principles" representations of the multidimensional dipole moment and polarizability of water that enable molecular-level investigations of IR and Raman spectra at a fully quantum-mechanical level. Our contribution builds upon the observation that the dipole moment and polarizability of a molecular system can rigorously be calculated through derivatives of the system's energy with respect to external electric fields,[77] which thus allows one to derive formally exact many-body expansions of the dipole moment and polarizability. The article is organized as follows: in Section 2, we describe the theoretical and technical details associated with the development of many-body representations of the dipole moment and polarizability for water. In Section 3, we demonstrate that these MB representations are capable of accurately describing the dipole moment and polarizability of water systems in both gas and condensed phases. Finally, we combine the newly developed many-body dipole moment and polarizability surfaces with CMD simulations carried out with our many-body MB-pol potential to model both IR and Raman spectra of liquid water under ambient conditions. A brief summary and outlook is given in Section 4.

2. METHODS

Within the many-body formalism, the total dipole moment of a molecular system can be expressed as

$$\mu_\alpha^{N\text{-mer}}(1,...,N) = \sum_i^N \mu_\alpha^{1B}(i) + \sum_{i,j}^N \mu_\alpha^{2B}(i,j) + ... + \mu_\alpha^{NB}(1,...,N) \tag{5}$$

where μ^{nB} is the nth interaction-induced dipole term and the subscript Greek letters are the Cartesian tensor indices. An analogous expression can be written for the system polarizability

$$\alpha_{\alpha\beta}^{N\text{-mer}}(1,...,N) = \sum_i^N \alpha_{\alpha\beta}^{1B}(i) + \sum_{i,j}^N \alpha_{\alpha\beta}^{2B}(i,j) + ... + \alpha_{\alpha\beta}^{NB}(1,...,N) \tag{6}$$

where α^{nB} is now the nth interaction-induced polarizability. In ref 78, we established the convergence of eqs 5 and 6 for water clusters of different sizes and demonstrated that, for these systems, the dipole moment and polarizability are dominated by 1B and 2B contributions, with higher-order terms contributing less than 4%. Unlike the interaction energy, where 3B terms make a substantial contribution,[79−87] the more rapid convergence of eqs 5 and 6 suggests that accurate representations of the dipole moment and polarizability surfaces for water can focus on 1B and 2B contributions only, allowing 3B and higher-order terms to be treated in an effective way (or neglected entirely, depending on the desired level of accuracy). Importantly, as discussed in ref 78, an explicit description of the 2B term is required to correctly capture electronic quantum-mechanical effects arising from exchange and charge transfer,[88−90] which play an important role at short-range and are neglected in purely polarizable models.

Exploiting eqs 5 and 6 and building upon our previous results,[78] we introduce here many-body representations of the dipole moment (MB-μ) and polarizability (MB-α) surfaces for water derived from highly correlated electronic structure calculations. The 2B terms were fit to 2B dipoles and polarizabilities calculated for 42 495 configurations defined in ref 56 at the RI-MP2/aug-cc-pVTZ level using the counterpoise method to correct for the basis set superposition error (BSSE).[91] It was previously demonstrated by us that this level of theory accurately describes 2B electrostatic properties of water.[78] Both dipole moment and polarizability were calculated through finite field calculations with an electric field of 0.005 au[92] using Molpro (version 2012.1).[93]

MB-μ is constructed as a sum of explicit 1B and 2B terms, with higher-order terms being described through many-body polarization. Specifically, the 1B term corresponds to the LTP2011 dipole moment surface developed by Lodi et al.,[94] which was fitted to the water molecular dipole obtained from all-electron, internally contracted multireference configuration interaction calculations in the aug-cc-pV6Z basis set, including corrections for size-extensivity and relativistic effects. The 2B dipole moment is modeled through two distance-dependent contributions. In the long-range region, where two water molecules are well-separated, the total dipole moment is represented through classical electrostatic interactions ($\mu^{2B,ind}$) described by the Thole-type point polarizable dipole model of Burnham and co-workers,[67] with minor modifications described in ref 56 and referred to here as TTM4-Ind. At short-range, where the electron densities of the individual monomers overlap, permutationally invariant polynomials are used to correctly capture the complexity of electronic quantum-mechanical effects contributing to the 2B dipole moment ($\mu^{2B,poly}$),

$$\mu_\alpha^{2B}(i,j) = s_2(t(r_{OO}))\mu_\alpha^{2B,poly}(i,j) + [1 - s_2(t(r_{OO}))]\mu_\alpha^{2B,ind}(i,j) \tag{7}$$

Here, $s(t(r_{OO}))$ is a switching function that smoothly transitions from 1 to 0 as a molecule is moved from the short-range to the long-range region, with the range of the transition region being controlled by $t(r) = \frac{r - R_i}{R_o - R_i}$. The inner and outer limits of the transition region, R_i and R_o, correspond to 5.5 and 7.5 Å, respectively. The explicit form of the switching function is given by

$$s_2(x) = \begin{cases} 1 & \text{if } x < 0 \\ 1 + x^2(2x - 3) & \text{if } 0 \le x < 1 \\ 0 & \text{if } x \le 1 \end{cases} \tag{8}$$

The short-range dipole moment is represented as a sum over atom-centered effective charges multiplied by the corresponding Cartesian positions of the atoms

$$\mu_\alpha^{2B} = \sum_i^6 q^i(\xi_0^\mu, ..., \xi_{14}^\mu) r_\alpha^i \tag{9}$$

The effective charges depend on the internal geometry of the water dimer through the auxiliary variables, ξ, which are formed from the exponentiated interatomic distances, e^{-kr}, where k is a

DOI: 10.1021/ct501131j
J. Chem. Theory Comput. 2015, 11, 1145−1154

parameter controlling the range of the exponent and r is the interatomic distance as shown in the Supporting Information. These auxiliary variables are used to form polynomials that are invariant with respect to permutation of all other like atoms and covariant when permuted with any other like atom. A more complete description of the symmetrization procedure can be found in the Appendix of ref 64. Importantly, to ensure invariance of the dipole moment upon changes of the origin, the sum of the effective charges was constrained to zero during the fitting. Because charge neutrality is achieved only within a given tolerance (in this study, an RMS error of 10^{-6} charge units), each dimer was positioned such that the oxygen−oxygen (O−O) center of mass was located at the origin of the reference frame. This was enforced both during the fitting and the evaluation of the 2B dipole. The charges, q^i, in eq 9 are described in terms of fifth order polynomials in the auxiliary variables presented in Table S1, resulting in 1826 terms for q^{H} and 1052 for q^{O}. The linear coefficients of the polynomials were fitted with singular value decomposition, whereas the six nonlinear parameters describing the range of the auxiliary variables were optimized using the simplex algorithm, with the least-squares solution solved at each iteration, as described in ref 56. For the 2B dipole, the six nonlinear parameters were those controlling the range of the auxiliary variables ($k^{\mathrm{O}}_{\mathrm{OO}}$, $k^{\mathrm{O}}_{\mathrm{OH}}$, $k^{\mathrm{O}}_{\mathrm{HH}}$, $k^{\mathrm{H}}_{\mathrm{OO}}$, $k^{\mathrm{H}}_{\mathrm{OH}}$, $k^{\mathrm{H}}_{\mathrm{HH}}$), where the superscript indicates the effective charge to which the variable contributes and the subscript indicates the atom pair that forms the distance. All higher-order terms of MB-μ are described by the TTM4-Ind model.[56,67] For the training set of 42 495 2B dipoles moments, the RMS error is 0.01 D. When restricting the set to the ∼32 000 dimers with binding energies less than 25 kcal/mol, the RMS error is 0.003 D. A correlation plot of the fit with respect to the training set is presented in Figure S1 of the Supporting Information.

Similarly to MB-μ, the many-body representation of the water polarizability (MB-α) is described as a sum of explicit 1B and 2B contributions, and a many-body term defined as

$$\alpha_{\alpha\beta}^{N\text{-mer}}(1,...,N) = \sum_{i}^{N} \alpha_{\alpha\beta}^{1\mathrm{B}}(i) + \sum_{i,j}^{N} \alpha_{\alpha\beta}^{2\mathrm{B}}(i,j) + \alpha_{\alpha\beta}^{\mathrm{MB}}(1,...,N) \tag{10}$$

Here, $\alpha_{\alpha\beta}^{1\mathrm{B}}$ is the 1B polarizability model of Avila, which was fitted to molecular polarizabilities calculated at the CCSD level.[95] Unlike the 2B term of the dipole moment, the short-range 2B contribution to the polarizability was directly built on top of the TTM4-Ind polarizability. The 2B polarizability thus takes the form

$$\alpha_{\alpha\beta}^{2\mathrm{B}}(i,j) = s_2(t(r_{\mathrm{OO}}))\alpha_{\alpha\beta}^{2\mathrm{B,poly}}(i,j) + \alpha_{\alpha\beta}^{2\mathrm{B,ind}}(i,j) \tag{11}$$

where the switching function again turns off the short-range 2B polynomial over a transition region from 5.5 to 7.5 Å. The short-range 2B term is represented by effective isotropic polarizabilities, α^i, which are cast into the lab frame by multiplication by the unit vectors, $\hat{\epsilon}^i$, associated with the sites carrying the effective polarizabilities

$$\alpha_{\alpha\beta}^{2\mathrm{B,poly}} = \sum_{i}^{10} \alpha^i(\chi_0^\alpha, ..., \chi_3^\alpha 0)\hat{\epsilon}_\alpha^i\hat{\epsilon}_\beta^i \tag{12}$$

This functional form has the advantage of generating a symmetric polarizability tensor. The invariance of the polarizability with respect to the choice of origin is achieved by centering the O−O centroid of the dimer at the origin. Importantly, unlike the dipole moment, where the effective charges were placed only on the atomic sites, the effective polarizabilities are positioned on both the three atomic sites and two additional lone-pair sites of each molecule. As in ref 56, the two lone-pair positions are defined by

$$\boldsymbol{r}_{\mathrm{L}}^{\pm} = \boldsymbol{r}_{\mathrm{O}} + \frac{1}{2}\gamma_{\parallel}(\boldsymbol{r}_{\mathrm{OH}_1} + \boldsymbol{r}_{\mathrm{OH}_2}) \pm \gamma_{\perp}[\boldsymbol{r}_{\mathrm{OH}_1} \times \boldsymbol{r}_{\mathrm{OH}_2}] \tag{13}$$

The parameters $\gamma_{\parallel}$ and $\gamma_{\perp}$ determine the position of the lone pair and were optimized during the fitting process. The effective polarizabilities are represented by polynomials formed from auxiliary variables depending on the interatomic distances (Table S1), maintaining the same in-/covariant properties as for the dipole moment. Due to the larger number of possible interatomic distances, the exponential range parameters were assumed to be the same regardless of the effective polarizability (i.e., $k^{\mathrm{O}}_{ab} = k^{\mathrm{H}}_{ab} = k^{\mathrm{L}}_{ab}$). This results in the following nonlinear parameters: k_{OO}, k_{OH}, k_{OL}, k_{HH}, k_{HL}, k_{LL}, $\gamma_{\parallel}$, and $\gamma_{\perp}$. Third-degree polynomials, composed of 435 terms for α^{O}, 603 terms for α^{H}, and 588 terms for α^{L}, were found to accurately fit the reference data, with a RMS error of 0.03 Å^3 over the entire training set and 0.009 Å^3 for dimers with binding energy less than 25 kcal/mol. In the same way as for MB-μ, all higher-order terms in MB-α are represented through the many-body polarizability arising from the TTM4-Ind model.[56,67]

3. RESULTS

3.1. Electrostatic Properties of Clusters. Since MB-μ and MB-α correctly reproduce the reference dipole moment and polarizability of the corresponding training sets, their transferability is tested here on small water clusters. Specifically, we compare the 2B dipole moment and polarizability predicted by MB-μ and MB-α for 14 water clusters containing from four to six molecules against reference values obtained at the RI-MP2/aug-cc-pVTZ level of theory including the counterpoise correction for BSSE. Figure 1 shows the RMS error in the dipole moment (panel a) and polarizability (panel b) obtained for different (electrostatics) models, including TTM4-Ind, WHBB, and the present many-body representations, MB-μ and MB-α. In these comparisons, TTM4-Ind refers to the polarizable model derived from the TTM4-F water potential that MB-μ and MB-α are built upon, whereas WHBB is the model of refs 41 and 64 in which the total dipole is expressed as a sum of 1B and 2B contributions only. Following our previous analysis of the electrostatic properties of water clusters,[78] the RMS errors shown in Figure 1 for each model were calculated as

$$\|\boldsymbol{p}^{\mathrm{MP2}} - \boldsymbol{p}^{\mathrm{model}}\|_{\mathrm{F}} \tag{14}$$

where $\boldsymbol{p}$ is either the dipole moment or the polarizability. The absolute values of the dipole moment and polarizability calculated for each cluster at the RI-MP2/aug-cc-pVTZ level of theory are also shown in Figure 1a,c, respectively, as a reference.

MB-μ and MB-α clearly provide a significant improvement upon the underlying, purely induced-electrostatics model (TTM4-ind), with an error in the 2B properties of at most 5 and 6% for the dipole moment and polarizability, respectively. Since both MB-μ and WHBB are built within the same theoretical framework, they would be expected to be able to describe the 2B dipole moment of water clusters with similar

DOI: 10.1021/ct501131j
J. Chem. Theory Comput. 2015, 11, 1145−1154

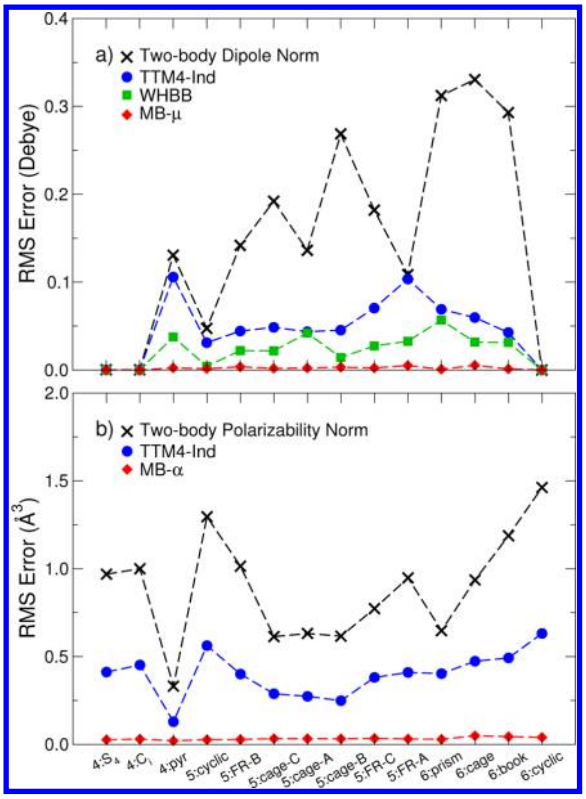

Figure 1. Ability of different models for the dipole moment and polarizability to reproduce the two-body electrostatic properties for clusters ranging from four to six water molecules. On the x axis is the isomer index, corresponding to the clusters of refs 96 and 97, where the first number indicates the number of water molecules in the cluster. (a) RMS error in the 2B dipole; (b) RMS error in the 2B polarizability. The reference electronic structure method is RI-MP2/aug-cc-pVTZ with BSSE-correction.

accuracy. This suggests that the relatively larger RMS errors predicted by WHBB in Figure 1 compared to that by MB-μ likely arise from differences in the composition of the corresponding training sets as well as in the level of theory used in the calculations of the reference data. Specifically, the WHBB 2B dipole moment surface was derived from BSSE-uncorrected MP2/aug-cc-pVTZ dipole moments, whereas the reference data used to develop MB-μ were calculated including the counterpoise correction to remove the BSSE.

3.2. Comparison of Two-Body Properties from Liquid Simulations. Having established that MB-μ and MB-α correctly describe the dipole moment and polarizability of water clusters, the accuracy of both many-body surfaces is assessed here for liquid water. While reference data for the energetics of water systems under periodic boundary conditions have recently become available from quantum Monte Carlo calculations,[98,99] we are unaware of any benchmark calculations for the electrostatic properties of liquid water. For this reason, we investigate here the accuracy of MB-μ and MB-α in reproducing the dipole moment and polarizability of a hydrogen-bonded dimer along a 2 ps CMD trajectory extracted from a simulation of liquid water under ambient conditions.[58] During the course of the 2 ps trajectory, the distance between the oxygen atoms of the two water molecules within the dimer varies from 2.6 to 3.6 Å (with an average value of 3.15 Å), exploring a wide range of hydrogen-bond strengths. For each trajectory frame, reference 2B dipoles and polarizabilities were calculated at the RI-MP2/aug-cc-pVTZ level of theory including the counterpoise correction for BSSE. It is important to emphasize that none of the 1000 dimer configurations visited during the CMD trajectory were included in the training sets used for the development of both MB-μ and MB-α.

The fractional errors ($\|\boldsymbol{p}^{\mathrm{MP2}} - \boldsymbol{p}^{\mathrm{model}}\|_{\mathrm{F}}/\|\boldsymbol{p}^{\mathrm{MP2}}\|_{\mathrm{F}}$) associated with the dipole moment and polarizability calculated with different models, including four density functionals commonly used in water simulations (BLYP, B3LYP, PBE, and PBE0), are shown in Figure 2. All DFT calculations were carried out with

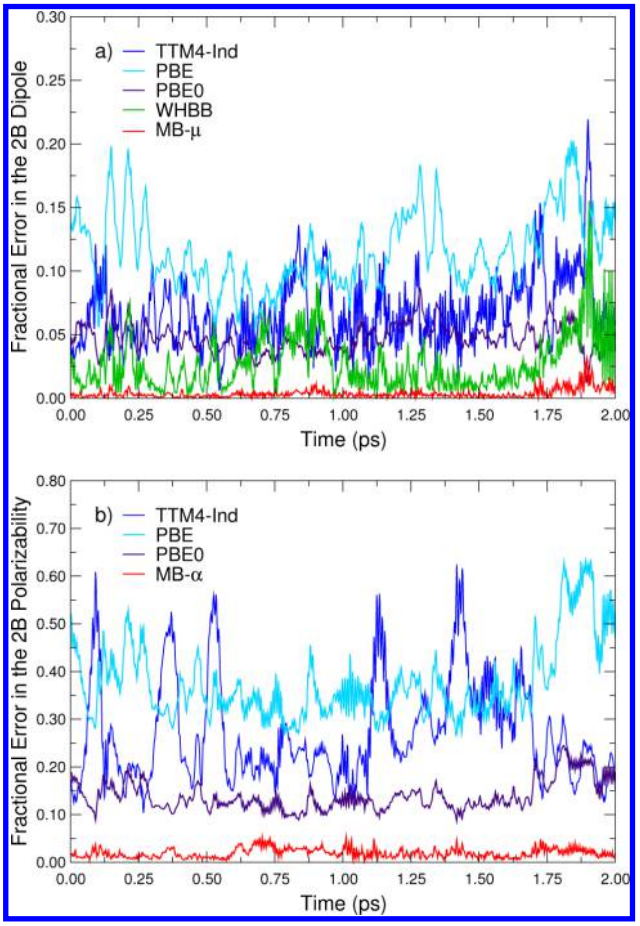

Figure 2. Fractional errors in the 2B dipole moments (a) and polarizabilities (b) are examined for hydrogen-bonded dimers extracted from a CMD simulation of liquid water. The reference properties were calculated at the RI-MP2/aug-cc-pVTZ level with BSSE correction. The properties obtained for PBE and PBE0 density functionals are also presented (obtained in the aug-cc-pVTZ basis with BSSE correction). Results for BLYP and B3LYP are shown in the Supporting Information.

the aug-cc-pVTZ basis and were corrected for BSSE using the counterpoise method. Given the similarity between the results obtained with BLYP and PBE and with B3LYP and PBE0, only the PBE and PBE0 fractional errors are included in Figure 2. Figures including the results of BLYP and B3LYP are reported in the Supporting Information.

Figure 2 clearly demonstrates that the 2B polarizability is more difficult to reproduce than the 2B dipole moment. Among all models considered here, MB-μ and MB-α provide the closest agreement with the reference data, with fractional errors of 0.4 and 2% in the 2B dipole moment and polarizability, respectively. GGA functionals (i.e., PBE and BLYP) have errors

DOI: 10.1021/ct501131j
J. Chem. Theory Comput. 2015, 11, 1145−1154

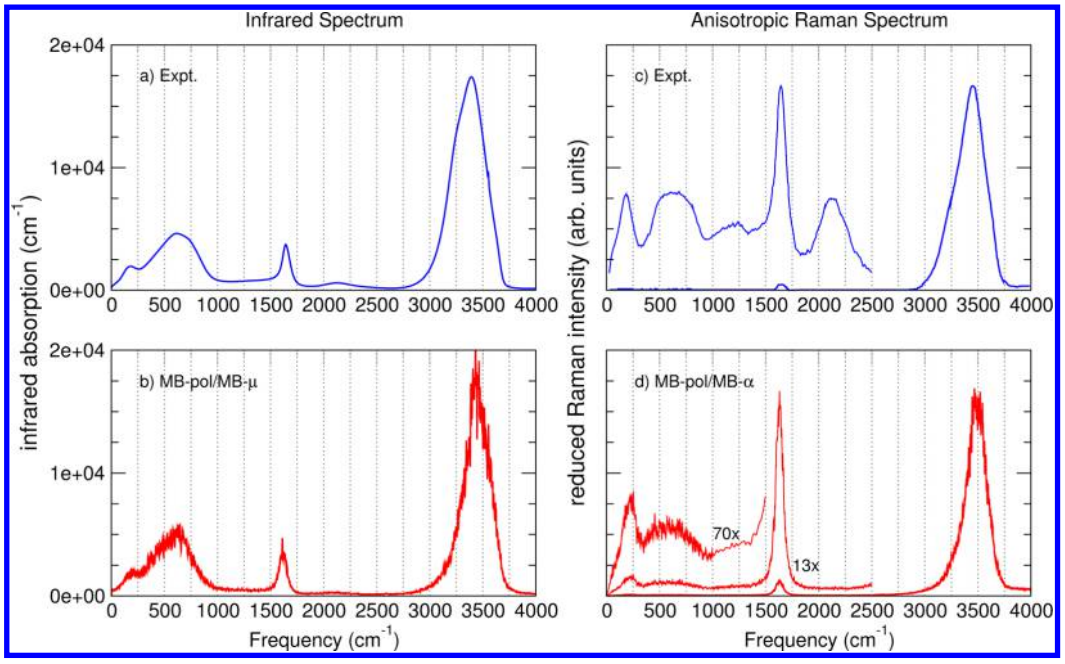

Figure 3. Experimental and simulated infrared (a, b) and reduced anisotropic Raman spectra (c, d) are presented for liquid water under ambient conditions. To clearly demonstrate the line shape of the lower-frequency features in the Raman spectra, the features were magnified, as described in the text. The experiments in panels (a) and (c) are adapted from refs 102 and 101, respectively.

of ~20% for the dipole moments and more than 60% for the polarizabilities. Compared to the GGA functionals, hybrid functionals predict relatively smaller fractional errors for all configurations visited along the CMD trajectory, which suggests that inclusion of Hartree−Fock exchange is likely important for correctly describing the electrostatic properties of liquid water.

3.3. Vibrational Spectra of Liquid Water. Given the accuracy of our MB-pol, MB-μ, and MB-α models in describing the water interactions, dipole moment, and polarizability, respectively, these three surfaces were combined in CMD simulations of IR and (anisotropic) Raman spectra of liquid water under ambient conditions. The frequency dependence of the IR absorption coefficient, $\alpha(\omega)$, was calculated as

$$\alpha(\omega)n(\omega) = \left[\frac{2\omega}{3V\hbar c\epsilon_{vac}}\right]\tanh\left(\frac{\hbar\omega}{kT}\right)\int_{-\infty}^{\infty} dt\ e^{-i\omega t}\langle \boldsymbol{\mu}(0)\boldsymbol{\mu}(t)\rangle \quad (15)$$

where V is the volume of the simulation cell, c is the speed of light, $n(\omega)$ is the frequency dependent refractive index of the system, and $\langle \boldsymbol{\mu}(0)\boldsymbol{\mu}(t)\rangle$ is the quantum dipole autocorrelation function.[31] The anisotropic reduced Raman spectrum was obtained through

$$R(\omega) = \frac{2\omega}{(\omega_I - \omega)^4}\tanh\left(\frac{\hbar\omega}{kT}\right)\int_{-\infty}^{\infty} dt\ e^{-i\omega t}\langle \mathrm{Tr}[\boldsymbol{\beta}(0)\boldsymbol{\beta}(t)]\rangle \quad (16)$$

where $\boldsymbol{\beta}$ is the anisotropy of the dipole−dipole polarizability, obtained by removing the isotropic component of the polarizability tensor: $\boldsymbol{\beta}_{\alpha\beta} = \boldsymbol{\alpha}_{\alpha\beta} - 1/3\mathrm{Tr}[\boldsymbol{\alpha}]$.[31] MB-$\mu$ and MB-α were used to calculate the correlation functions appearing in eqs 15 and 16, and the nuclear quantum dynamics was approximated by adiabatic CMD using the MB-pol potential energy surface to describe the interactions between water molecules. Specifically, 10 CMD simulations were performed, each of which was 27 ps long and was seeded from different initial conditions obtained from PIMD simulations carried out at 298.15 K. The CMD propagation was performed in the normal-mode representation, and decoupling between the dynamics of the centroid and nonzero frequency normal modes was obtained with an adiabaticity parameter $\gamma = 0.1$.[36,100] A time step of 0.02 fs was found to be sufficient for energy conservation. To enable the study of local solvation dynamics, instead of simulating pure H_2O, a single HOD molecule was placed in 215 H_2O molecules. In this very low concentration, the HOD molecule is expected to have negligible effect on the calculated vibrational spectra (indeed, no OD stretch or HOD bend is discernible in the calculated spectra).

The IR and Raman spectra calculated using our MB-MD approach are compared with the corresponding experimental results in Figure 3. The reduced anisotropic Raman spectra (Figure 3c,d) are presented in arbitrary units, with the experimental spectrum being adapted from ref 101. Due to the use of arbitrary units in the experimental results, the Raman spectrum was normalized to the maximum intensity of the OH stretch, with successive levels of magnification employed for the bend and the low-frequency features. Examination of the low-frequency features of the IR and Raman indicates that MB-pol provides an accurate description of the hydrogen-bonding dynamics. The maximum of the calculated librational band (the broad feature between 400 and 800 cm^{-1} that is related to the hindered reorientation of molecules due to intermolecular interactions) lies within a few wavenumbers of the corresponding experimental value. In addition, the frequency of hydrogen-bond stretches (~180 cm^{-1}) is also in very good agreement with experiment. For the Raman spectra, the agreement between simulation and experiment is somewhat less good, with the position of hydrogen-bond stretches being slightly blue shifted and the tapered plateau of the librations being less

DOI: 10.1021/ct501131j
J. Chem. Theory Comput. 2015, 11, 1145−1154

defined. As is apparent in Figure 3, some imbalance in the relative intensities of the stretch, bend, and librations is also present in the calculated Raman spectrum compared to the experimental results. Given the good agreement between the calculated and measured IR spectra, which implies that the underlying (quantum) molecular dynamics is correctly described, and the high accuracy of the 1B and 2B polarizabilities, the differences found between the calculated and experimental Raman spectra suggests that effects neglected by MB-α may be important for the low-frequency Raman spectra, such as higher-order many-body effects, frequency dependence of the polarizability, or higher-order polarizability. In addition, the association band around 2250 cm^{-1} (arising from the combination of librational modes with the bending vibration) is barely visible in the IR spectrum and is missing in the Raman spectrum. It has been suggested that this feature, which may partially be recovered in the local monomer approximation,[36] may not be completely captured through approximate quantum dynamics methods such as CMD.

The position of the OH stretch feature has proven to be quite difficult to reproduce theoretically due to its anharmonicity and highly quantum-mechanical nature. For instance, empirically parametrized fixed-charge water models typically struggle to capture the average position of the OH band and predict shape and intensity (even after inclusion of quantum correction factors) that are significantly different from the experimental measurements.[103,104] Inclusion of polarization effects improves the agreement, particularly in the intensity,[66−68,70] although empirical parametrizations are often still required to correctly predict the position of the OH band. More recently, *ab initio* molecular dynamics simulations have also been employed to model vibrational spectra. Classical MD simulations with GGA functionals predict strongly red-shifted bands (upon which nuclear quantum effects can be expected to lead to an additional redshift of 100−150 cm^{-1}).[72−74] Somewhat better results were obtained with hybrid functionals, although both position and intensity of the OH stretch band are generally not well reproduced.[75] The position of the OH stretch band predicted by our MB-MD approach is in good agreement with the corresponding experimental results, with the intensity maxima being slightly shifted to the blue by roughly 40 and 30 cm^{-1} in the IR and Raman spectra, respectively. However, the shape of both the calculated IR and Raman OH bands is somewhat skewed. In particular, while both the onset 2850 cm^{-1} and the position and shape of the blue side of the band are in good agreement with experiment, the low-frequency portion of the band is lacking in intensity.

To understand the origin of the missing stretch intensity, it is important to consider the interplay between the bend and stretch bands. With a maximum at ∼1640 cm^{-1} in both IR and Raman experimental spectra, the bend overtone lies squarely within the OH stretching region. For this reason, it has long been proposed that a Fermi resonance may exist in liquid water between the bend overtone and the OH stretch fundamental, contributing additional intensity to the signal in the strongly H-bonded stretch region. Therefore, in order to correctly reproduce the shape of the OH stretch band, (1) the bending frequency must be correctly positioned such that its overtone coincides with the stretch fundamental and (2) the dynamical method must be able to describe the Fermi resonance between the two vibrational modes. While the extent to which CMD can capture Fermi resonances is unclear, the present situation is undoubtedly complicated by the fact that the water bend is slightly red-shifted with respect to experiment, by 28 and 14 cm^{-1} for the IR and Raman spectra, respectively. Given the overall good agreement between the calculated and experimental bending frequency and similar baselines for the calculated and experimental OH bands, it thus seems plausible that the lack of intensity in the red portion of the calculated OH band may be due to quantum dynamical effects associated with the Fermi resonance rather than to missing hydrogen-bonded configurations.

3.4. Characterizing the Stretch Line Shape. To provide further insights into the origin of the OH line shape, the contributions of the potential energy surface and the Fermi resonance are isolated by studying the vibrationally decoupled OD stretch of the dilute HOD molecule in H_2O. Due to the difference in molecular mass, the bend overtone of HOD lies outside the OH stretch band, removing the effect of the Fermi resonance. In addition, because the O−O radial distribution function given by MB-pol is in excellent agreement with the experimental data, this suggests that the differences in the vibrational structure between simulations and experiment are likely associated with the distribution of the hydrogen atoms, which can be efficiently probed by focusing on the OD vibrational frequencies of HOD in H_2O. Therefore, this isotopically dilute system is ideally situated to disentangle dynamical effects from the underlying potential energy landscape.

To assess the accuracy of MB-pol in describing the OD vibrational frequencies of the HOD molecule in H_2O, QM/MM calculations at the MP2/cc-pVTZ level were performed for 2500 cluster configurations extracted from a 10 ps CMD simulation of HOD in H_2O. Following the procedure outlined by the Skinner group,[44] water molecules were assigned to the QM region if their oxygen atoms were within 4.2 Å of the deuterium atom of the central HOD molecule. In addition to these QM H_2O molecules, a-SPC/Fw partial charges placed on the next closest 80 molecules were included in the MM region.[105] For each cluster configuration, the fully anharmonic OD transition frequency from the $v = 0$ to the $v = 1$ energy level was obtained by calculating the potential energy curves associated with the OD stretch and solving the corresponding one-dimensional vibrational Schrödinger equation. Analogous QM/MM calculations were carried out using MB-pol to describe the QM region. The resulting frequency distributions are shown in Figure 4.

The comparison clearly shows that the frequencies obtained from MB-pol and MP2 are effectively identical. The frequency distributions cannot be compared directly to the OD IR or Raman line shape because they lack dynamical effects (e.g., motional narrowing and non-Condon effects[50,51,106]), which are known to red shift and narrow the underlying distribution. Nonetheless, the close agreement between MB-pol and MP2 provides further evidence that the MB-pol is comparable in accuracy with correlated electronic structure methods, suggesting that the origin of the differences between the calculated and experimental spectra in the OH region lies elsewhere. To enumerate possible sources of differences, we first note that the intramolecular geometry of water molecules in the liquid may be (slightly) different for MB-pol and MP2, resulting in (slightly) different OH vibrational frequencies. These differences cannot be identified in the QM/MM calculations, which probe only one of the intramolecular degrees of freedom. To test this hypothesis, CMD simulations at the MP2 [and possibly CCSD(T)] levels should be carried out. Unfortunately,

DOI: 10.1021/ct501131j
J. Chem. Theory Comput. 2015, 11, 1145−1154

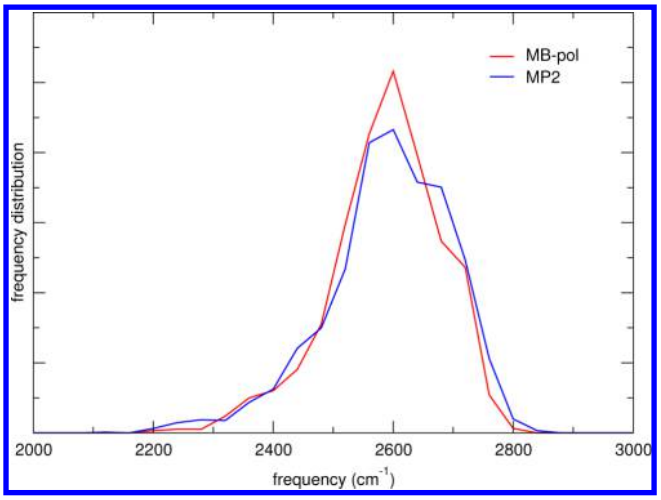

Figure 4. OD frequency distributions of dilute HOD in H_2O obtained from QM/MM calculations with MB-pol (red) and MP2/cc-pVTZ (blue) used in the QM region.

despite much recent progress,[107] such simulations are currently out of reach. Second, an exact treatment of nuclear quantum dynamics is required to rigorously capture the nature of the OH stretch band. While not yet possible, this is also an active area of research.[108] Finally, the differences may arise from intrinsic limitations of current, state-of-the-art electronic structure methods from which the many-body surfaces are derived.[109,110]

4. SUMMARY

Accurately modeling vibrational spectra from first principles requires a robust treatment of quantum dynamical effects, a potential energy surface that gives rise to the vibrational motion of the system, and a faithful description of the dipole moment and polarizability as a function of the system's degrees of freedom (which determine the IR and Raman activity of the underlying vibrations, respectively). Here, we developed "first-principles" models for the dipole moment (MB-μ) and polarizability (MB-α) of water by exploiting the rapid convergence of the many-body expansion of interactions. Centroid molecular dynamics simulations were used to simulate the quantum dynamics of liquid water under ambient conditions using the MB-pol PES. Using MB-μ and MB-α to evaluate the dipole and polarizability time correlation functions, it was found that the both the positions and intensities of the infrared and Raman spectral features are in good agreement with experiment, without relying on any *ad hoc* parameters. While the overall position and intensity of the OH vibrational band are accurate, the line width is somewhat too narrow, lacking intensity on the red side.

To provide insights into the origin of the OH line shape, QM/MM calculations of dilute HOD in H_2O were carried out using MB-pol and MP2 in the QM region. The close agreement between the OD frequency distributions obtained at the MB-pol and MP2 levels provides further evidence for the accuracy of MB-pol. This also suggests that the differences between the calculated and experimental spectra may be due to inherent limitations in the electronic structure methods (even at the correlated level)[109,110] and/or an incomplete description of the nuclear quantum dynamics (e.g., combination bands and Fermi resonances). Given that MB-pol, MB-μ, and MB-α are built purely from first principles and provide good agreement with correlated electronic structure calculations, this analysis suggests that empirical models that provide the correct OH line width for H_2O using MD or CMD simulations may benefit from unphysical compensation of effects, artificially encoding quantum dynamical effects into the empirically parametrized interactions. While improvements to electronic structure and quantum dynamics methods may be necessary to quantitatively capture subtle, quantum mechanical effects, the many-body molecular dynamics (MB-MD) approach introduced here represents a powerful "first-principles" method for the study of vibrational spectroscopy.

■ ASSOCIATED CONTENT

Supporting Information

Scatter plots of the fitted models of the 2B dipole and polarizability versus the respective training sets and results from BLYP and B3LYP for the 2B dipoles and polarizabilities of the dimer extracted from the CMD simulation of liquid water. This material is available free of charge via the Internet at http://pubs.acs.org.

■ AUTHOR INFORMATION

Corresponding Author

*E-mail: fpaesani@ucsd.edu.

Funding

This research was supported by the National Science Foundation Center for Chemical Innovation "Center for Aerosol Impacts on Climate and the Environment" (grant CHE-1305427). This work used the Extreme Science and Engineering Discovery Environment (XSEDE), which is supported by the National Science Foundation grant no. ACI-1053575 (allocation TG-CHE110009). G.R.M. acknowledges the Department of Education for support through the GAANN fellowship program.

Notes

The authors declare no competing financial interest.

■ ACKNOWLEDGMENTS

We thank Professor Tauber for helpful discussions regarding the interpretation of the Raman spectra.

■ REFERENCES

(1) Maréchal, Y. *The Hydrogen Bond and the Water Molecule: The Physics and Chemistry of Water, Aqueous and Bio-Media*; Elsevier: Amsterdam, 2006.
(2) Ault, A. P.; Guasco, T. L.; Ryder, O. S.; Baltrusaitis, J.; Cuadra-Rodriguez, L. A.; Collins, D. B.; Ruppel, M. J.; Bertram, T. H.; Prather, K. A.; Grassian, V. H. *J. Am. Chem. Soc.* **2013**, *135*, 14528−14531.
(3) Tobias, D. J.; Stern, A. C.; Baer, M. D.; Levin, Y.; Mundy, C. J. *Annu. Rev. Phys. Chem.* **2013**, *64*, 339−59.
(4) Hopkins, A. J.; McFearin, C. L.; Richmond, G. L. J. *Phys. Chem. C* **2011**, *115*, 11192.
(5) Jubb, A. M.; Hua, W.; Allen, H. C. *Annu. Rev. Phys. Chem.* **2012**, *63*, 107−130.
(6) DeFlores, L. P.; Tokmakoff, A. *J. Am. Chem. Soc.* **2006**, *128*, 16520−16521.
(7) Ebbinghaus, S.; Kim, S. J.; Heyden, M.; Yu, X.; Heugen, U.; Gruebele, M.; Leitner, D. M.; Havenith, M. *Proc. Natl. Acad. Sci. U.S.A.* **2007**, *104*, 20749−52.
(8) Szyc, L.; Yang, M.; Nibbering, E. T. J.; Elsaesser, T. *Angew. Chem., Int. Ed.* **2010**, *49*, 3598−3610.
(9) Gruenbaum, S. M.; Skinner, J. L. *J. Chem. Phys.* **2011**, *135*, 075101.
(10) Canivet, J.; Fateeva, A.; Guo, Y.; Coasne, B.; Farrusseng, D. *Chem. Soc. Rev.* **2014**, *43*, 5594−5617.

DOI: 10.1021/ct501131j
J. Chem. Theory Comput. 2015, 11, 1145−1154

(11) Bourrelly, S.; Moulin, B.; Rivera, A.; Maurin, G.; Devautour-Vinot, S.; Serre, C.; Devic, T.; Horcajada, P.; Vimont, A.; Clet, G.; Daturi, M.; Lavalley, J.-C.; Loera-Serna, S.; Denoyel, R.; Llewellyn, P. L.; Férey, G. *Moulin* **2010**, *132*, 9488−9498.
(12) Keutsch, F. N.; Saykally, R. J. *Proc. Natl. Acad. Sci. U.S.A.* **2001**, *98*, 10533−10540.
(13) Fayer, M. D.; Levinger, N. E. *Annu. Rev. Anal. Chem.* **2010**, *3*, 89−107.
(14) Horvath, S.; McCoy, A. B.; Elliott, B. M.; Weddle, G. H.; Roscioli, J. R.; Johnson, M. A. *J. Phys. Chem. A* **2010**, *114*, 1556−68.
(15) Perakis, F.; Borek, J. A.; Hamm, P. *J. Chem. Phys.* **2013**, *139*, 014501.
(16) Medders, G. R.; Paesani, F. *J. Phys. Chem. Lett.* **2014**, *5*, 2897−2902.
(17) Nihonyanagi, S.; Ishiyama, T.; Lee, T.; Yamaguchi, S.; Bonn, M.; Morita, A.; Tahara, T. *J. Am. Chem. Soc.* **2011**, *133*, 16875−16880.
(18) Piatkowski, L.; Zhang, Z.; Backus, E. H. G.; Bakker, H. J.; Bonn, M. *Nat. Commun.* **2014**, *5*, 4083.
(19) Millo, A.; Raichlin, Y.; Katzir, A. *Appl. Spectrosc.* **2005**, *59*, 460−466.
(20) Smit, W. J.; Bakker, H. J. *J. Chem. Phys.* **2013**, *139*, 204504.
(21) McCoy, A. B. *J. Chem. Phys. B* **2014**, *118*, 8286−8294.
(22) Shen, Y. R.; Ostroverkhov, V. *Chem. Rev.* **2006**, *106*, 1140−1154.
(23) Skinner, J. L.; Pieniazek, P. A.; Gruenbaum, S. M. *Acc. Chem. Res.* **2012**, *45*, 93−100.
(24) Stiopkin, I. V.; Weeraman, C.; Pieniazek, P. A.; Shalhout, F. Y.; Skinner, J. L.; Benderskii, A. V. *Nature* **2011**, *474*, 192−195.
(25) Vinaykin, M.; Benderskii, A. V. *J. Phys. Chem. Lett.* **2012**, *3*, 3348−3352.
(26) Nagata, Y.; Hsieh, C.-S.; Hasegawa, T.; Voll, J.; Backus, E. H. G.; Bonn, M. *J. Phys. Chem. Lett.* **2013**, *4*, 1872−1877.
(27) Mukamel, S. *Principles of Nonlinear Optical Spectroscopy*; Oxford University Press: Oxford, 1995.
(28) Nitzan, A. *Chemical Dynamics in Condensed Phases: Relaxation, Transfer and Reactions in Condensed Molecular Systems*; Oxford University Press: Oxford, 2006.
(29) Bosma, W. B.; Fried, L. E.; Mukamel, S. *J. Chem. Phys.* **1993**, *98*, 4413.
(30) Saito, S.; Ohmine, I. *J. Phys. Chem.* **1995**, *102*, 3566.
(31) Iuchi, S.; Morita, A.; Kato, S. *J. Phys. Chem. B* **2002**, *106*, 3466−3476.
(32) Heyden, M.; Sun, J.; Funkner, S.; Mathias, G.; Forbert, H.; Havenith, M.; Marx, D. *Proc. Natl. Acad. Sci. U.S.A.* **2010**, *107*, 12068−73.
(33) Wan, Q.; Spanu, L.; Galli, G. A.; Gygi, F. *J. Chem. Theory Comput.* **2013**, *9*, 4124−4130.
(34) Hamm, P. *J. Chem. Phys.* **2014**, *141*, 184201.
(35) Ramírez, R.; López-Ciudad, T.; Kumar, P.; Marx, D. *J. Chem. Phys.* **2004**, *121*, 3973−3983.
(36) Rossi, M.; Liu, H.; Paesani, F.; Bowman, J.; Ceriotti, M. *J. Chem. Phys.* **2014**, *141*, 181101.
(37) Jansen, T. L. C.; Zhuang, W.; Mukamel, S. *J. Chem. Phys.* **2004**, *121*, 10577−10598.
(38) Choi, J.-H.; Hahn, S.; Cho, M. *Int. J. Quantum Chem.* **2005**, *104*, 616−634.
(39) Buch, V.; Tarbuck, T.; Richmond, G. L.; Groenzin, H.; Li, I.; Shultz, M. J. *J. Chem. Phys.* **2007**, *127*, 204710.
(40) Skinner, J. L.; Auer, B. M.; Lin, Y.-s. *Adv. Chem. Phys.* **2009**, *Vol. 142*, 59−103.
(41) Wang, Y.; Bowman, J. M. *J. Chem. Phys.* **2011**, *134*, 154510.
(42) Wang, Y.; Bowman, J. M. *J. Chem. Phys.* **2012**, *136*, 144113.
(43) Choi, J.-H.; Cho, M. *J. Chem. Phys.* **2013**, *138*, 174108.
(44) Auer, B.; Kumar, R.; Schmidt, J. R.; Skinner, J. L. *Proc. Natl. Acad. Sci. U.S.A.* **2007**, *104*, 14215−14220.
(45) Tainter, C. J.; Ni, Y.; Shi, L.; Skinner, J. L. *J. Phys.Chem. Lett.* **2013**, *4*, 12−17.
(46) De Marco, L.; Ramasesha, K.; Tokmakoff, A. *J. Phys. Chem. B* **2013**, *117*, 15319−27.
(47) Cao, J.; Voth, G. A. *J. Chem. Phys.* **1994**, *100*, 5106.
(48) Jang, S.; Voth, G. A. *J. Chem. Phys.* **1999**, *111*, 2357.
(49) Witt, A.; Ivanov, S. D.; Shiga, M.; Forbert, H.; Marx, D. *J. Chem. Phys.* **2009**, *130*, 194510.
(50) Paesani, F.; Voth, G. A. *J. Chem. Phys.* **2010**, *132*, 014105.
(51) Paesani, F.; Xantheas, S. S.; Voth, G. A. *J. Phys. Chem. B* **2009**, *113*, 13118−13130.
(52) Craig, I. R.; Manolopoulos, D. E. *J. Chem. Phys.* **2004**, *121*, 3368−3373.
(53) Habershon, S.; Fanourgakis, G. S.; Manolopoulos, D. E. *J. Chem. Phys.* **2008**, *129*, 074501.
(54) Rossi, M.; Ceriotti, M.; Manolopoulos, D. E. *J. Chem. Phys.* **2014**, *140*, 234116.
(55) Medders, G. R.; Babin, V.; Paesani, F. *J. Chem. Theory Comput.* **2013**, *9*, 1103−1114.
(56) Babin, V.; Leforestier, C.; Paesani, F. *J. Chem. Theory Comput.* **2013**, *9*, 5395−5403.
(57) Babin, V.; Medders, G. R.; Paesani, F. *J. Chem. Theory Comput.* **2014**, *10*, 1599−1607.
(58) Medders, G. R.; Babin, V.; Paesani, F. *J. Chem. Theory Comput.* **2014**, *10*, 2906−2910.
(59) Bukowski, R.; Szalewicz, K.; Groenenboom, G. C.; van der Avoird, A. *Science* **2007**, *315*, 1249−1252.
(60) Bukowski, R.; Szalewicz, K.; Groenenboom, G. C.; van der Avoird, A. *J. Chem. Phys.* **2008**, *128*, 094313.
(61) Bukowski, R.; Szalewicz, K.; Groenenboom, G. C.; van der Avoird, A. *J. Chem. Phys.* **2008**, *128*, 094314.
(62) Leforestier, C.; Szalewicz, K.; van der Avoird, A. *J. Chem. Phys.* **2012**, *137*, 014305.
(63) Góra, U.; Cencek, W.; Podeszwa, R.; van der Avoird, A.; Szalewicz, K. *J. Chem. Phys.* **2014**, *140*, 194101.
(64) Wang, Y.; Huang, X.; Shepler, B. C.; Braams, B. J.; Bowman, J. M. *J. Chem. Phys.* **2011**, *134*, 094509.
(65) Babin, V.; Medders, G. R.; Paesani, F. *J. Phys. Chem. Lett.* **2012**, *3*, 3765−3769.
(66) Fanourgakis, G. S.; Xantheas, S. S. *J. Chem. Phys.* **2008**, *128*, 074506.
(67) Burnham, C. J.; Anick, D. J.; Mankoo, P. K.; Reiter, G. F. *J. Chem. Phys.* **2008**, *128*, 154519.
(68) Mankoo, P. K.; Keyes, T. *J. Chem. Phys.* **2008**, *129*, 034504.
(69) Ishiyama, T.; Morita, A. *J. Chem. Phys.* **2009**, *131*, 244714.
(70) Hasegawa, T.; Tanimura, Y. *J. Phys. Chem. B* **2011**, *115*, 5545−5553.
(71) Silvestrelli, P. L.; Bernasconi, M.; Parrinello, M. *Chem. Phys. Lett.* **1997**, *277*, 478−482.
(72) Sharma, M.; Resta, R.; Car, R. *Phys. Rev. Lett.* **2005**, *95*, 187401.
(73) Lee, H.-S.; Tuckerman, M. E. *J. Chem. Phys.* **2007**, *126*, 164501.
(74) Chen, W.; Sharma, M.; Resta, R.; Galli, G.; Car, R. *Phys. Rev. B* **2008**, *77*, 245114.
(75) Zhang, C.; Donadio, D.; Gygi, F.; Galli, G. *J. Chem. Theory Comput* **2011**, *7*, 1443−1449.
(76) Vega, C. *Mol. Phys.* 2015; DOI: 10.1080/00268976.2015.1005191.
(77) Stone, A. J. *Theory of Intermolecular Forces*; Oxford University Press: Oxford, 1997.
(78) Medders, G. R.; Paesani, F. *J. Chem. Theory Comput.* **2013**, *9*, 4844−4852.
(79) Xantheas, S. S. *J. Chem. Phys.* **1994**, *100*, 7523−7534.
(80) Ojamie, L.; Hermansson, K. *J. Phys. Chem.* **1994**, *98*, 4271−4282.
(81) Pedulla, J. M.; Vila, F.; Jordan, K. D. *J. Chem. Phys.* **1996**, *105*, 11091.
(82) Hodges, M. P.; Stone, A. J.; Xantheas, S. S. *J. Phys. Chem. A* **1997**, *101*, 9163−9168.
(83) Xantheas, S. S. *Chem. Phys.* **2000**, *258*, 225−231.
(84) Cui, J.; Liu, H.; Jordan, K. D. *J. Phys. Chem. B* **2006**, *110*, 18872−18878.
(85) Hermann, A.; Krawczyk, R.; Lein, M.; Schwerdtfeger, P.; Hamilton, I.; Stewart, J. J. P. *Phys. Rev. A* **2007**, *76*, 013202.

DOI: 10.1021/ct501131j
J. Chem. Theory Comput. 2015, 11, 1145−1154

(86) Góra, U.; Podeszwa, R.; Cencek, W.; Szalewicz, K. *J. Chem. Phys.* **2011**, *135*, 224102.
(87) Khaliullin, R. Z.; Cobar, E. A.; Lochan, R. C.; Bell, A. T.; Head-Gordon, M. *Phys. Chem. Chem. Phys.* **2012**, *14*, 15328−15339.
(88) Szalewicz, K.; Cole, S. J.; Kołłos, W.; Bartlett, R. J. *J. Chem. Phys.* **1988**, *89*, 3662−3673.
(89) Chen, W.; Gordon, M. S. *J. Phys. Chem.* **1996**, *100*, 14316−14328.
(90) Khaliullin, R. Z.; Cobar, E. A.; Lochan, R. C.; Bell, A. T.; Head-Gordon, M. *J. Phys. Chem. A* **2007**, *111*, 8753−8765.
(91) Boys, S. F.; Bernardi, F. *Mol. Phys.* **1970**, *19*, 553.
(92) Kurtz, H. A.; Stewart, J. J. P.; Dieter, K. M. *J. Comput. Chem.* **1990**, *11*, 82−87.
(93) Werner, H.-J.; Knowles, P. J.; Knizia, G.; Manby, F. R.; Schütz, M.; et al. *MOLPRO*, version 2012.1, 2012; http://www.molpro.net.
(94) Lodi, L.; Tennyson, J.; Polyansky, O. L. *J. Chem. Phys.* **2011**, *135*, 034113.
(95) Avila, G. *J. Chem. Phys.* **2005**, *122*, 144310.
(96) Temelso, B.; Archer, K. A.; Shields, G. C. *J. Phys. Chem. A* **2011**, *115*, 12034−12046.
(97) Bates, D. M.; Tschumper, G. S. *J. Phys. Chem. A* **2009**, *113*, 3555−3559.
(98) Alfè, D.; Bartók, A. P.; Csányi, G.; Gillan, M. J. *J. Chem. Phys.* **2013**, *138*, 221102.
(99) Morales, M. A.; Gergely, J. R.; McMinis, J.; McMahon, J. M.; Kim, J.; Ceperley, D. M. *J. Chem. Theory Comput.* **2014**, *10*, 2355−2362.
(100) Hone, T. D.; Voth, G. A. *J. Chem. Phys.* **2004**, *121*, 6412.
(101) Brooker, M. H.; Hancock, G.; Rice, B. C.; Shapter, J. *J. Raman Spectrosc.* **1989**, *20*, 683−694.
(102) Bertie, J. E.; Lan, Z. *Appl. Spectrosc.* **1996**, *50*, 1047−1057.
(103) Paesani, F.; Zhang, W.; Case, D. A.; Cheatham, T. E.; Voth, G. A. *J. Chem. Phys.* **2006**, *125*, 184507.
(104) Habershon, S.; Markland, T. E.; Manolopoulos, D. E. *J. Chem. Phys.* **2009**, *131*, 024501.
(105) Park, K.; Lin, W.; Paesani, F. *J. Phys. Chem. B* **2012**, *116*, 343−352.
(106) Schmidt, J. R.; Corcelli, S. A.; Skinner, J. L. *J. Chem. Phys.* **2005**, *123*, 044513.
(107) Del Ben, M.; Schönherr, M.; Hutter, J.; VandeVondele, J. *J. Phys. Chem. Lett.* **2013**, *4*, 3753−3759.
(108) Makri, N. *J. Chem. Phys.* **2014**, *141*, 134117.
(109) Miliordos, E.; Aprà, E.; Xantheas, S. S. *J. Chem. Phys.* **2013**, *139*, 114302.
(110) Řezáč, J.; Hobza, P. *J. Chem. Theory Comput.* **2013**, *9*, 2151−2155.

DOI: 10.1021/ct501131j
J. Chem. Theory Comput. 2015, 11, 1145−1154